Impact of Subgrid-Scale Convection on Global Thermohaline Properties and Circulation

SEONG-JOONG KIM

Canadian Center for Climate Modelling and Analysis, University of Victoria, Victoria, British Columbia, Canada

ACHIM STÖSSEL

Department of Oceanography, Texas A&M University, College Station, Texas

(Manuscript received 6 August 1999, in final form 3 May 2000)

ABSTRACT

In most ocean general circulation models the simulated global-scale deep-ocean thermohaline properties appear to be chronically colder and fresher than observed. To some extent, this discrepancy has been known to be due to excessive open-ocean deep convection in the Southern Ocean (SO) caused by crude ''convective adjustment'' parameterizations on scales typically two orders of magnitude larger than the actual convection scale. To suppress the strength of open-ocean convection and to thereby eventually improve the global deep-ocean water properties, the authors first reduced convection in the SO in an ad hoc manner by activating it every 10 days rather than every model time step (20 hours). Second, a more physically based subgrid-scale convection in the SO was introduced by applying the penetrative plume convection scheme of Paluszkiewicz and Romea. With both treatments, SO convection decreased by about 30%, and the globally averaged deep-ocean potential temperature and salinity increased substantially to within 0.2°C and 0.02 psu of observed estimates. Furthermore, the plume convection scheme led to more realistic vertical temperature and salinity sections with more distinct Circumpolar Deep Water extension toward the south and a significant improvement of SO sea ice in terms of its thickness and its seasonality. The results of this study confirm that in order to obtain more realistic deep-ocean properties, open-ocean convection in the SO must be substantially weakened and shallower. This can be achieved by adopting a more physical plume convection scheme.

1. Introduction

The ocean plays a major role in the global climate system. Its large-scale and long-term impact is determined by the global overturning circulation, thermohaline properties, and meridional heat transports. Therefore, a reasonable reproduction of the world's deep-ocean properties is a critical issue in ocean general circulation models (OGCMs) to predict climate change (Broecker 1997). Unfortunately, most simulated deep-ocean water masses have shown a persistent discrepancy to observations. This has been attributed to an insufficient representation of oceanic convection, especially in the Southern Ocean (SO) (by, e.g., Duffy and Caldeira 1997; Duffy et al. 1999).

The world's deep-ocean water masses are mainly produced in a few scattered regions of the high latitudes through two types of convection mechanisms: open-ocean convection and near-boundary convection (Warren 1981; Killworth 1983; Marshall and Schott 1999, and references therein). Open-ocean deep convection, the predominant mechanism involved in the production of North Atlantic Deep Water (NADW), has been observed in the Greenland–Iceland–Norwegian (GIN) Sea, the Labrador Sea, and the northwestern Mediterranean Sea, while in the SO it seems to occur only occasionally (e.g., in the Weddell Polynya) (Marshall and Schott 1999, and references therein). On the other hand, near-boundary convection, which is the main process behind the production of Antarctic Bottom Water (AABW) occurs mostly at distinct locations around Antarctica (Killworth 1983, for a review). The Weddell Sea and the Ross Sea had been reported as the major AABW production region (Carmack 1977). Recently, Rintoul (1998) argued that actually more AABW is produced along the Adélie Land coast than in the Ross Sea.

The physics involved in these two convection mechanisms are different. In open-ocean deep convection, three phases are involved (Marshall and Schott 1999). First, a background cyclonic circulation is required as

Corresponding author address: Dr. Seong-Joong Kim, Canadian Center for Climate Modeling and Analysis, University of Victoria, MSC Post Office Box 1700, STN CSC, Victoria, BC V8W 2Y2, Canada.
E-mail: seong-joong.kim@ec.gc.ca

a ''preconditioning'' to raise the interior water to the surface. This is associated with doming of isopycnals. The surface proximity of dense water makes it more prone to instabilities than the surrounding waters. Second, ''deep convection'' is initiated by the loss of buoyancy due to intense surface cooling, often also involving brine rejection. Finally, ''lateral mixing'' occurs between the convection site and the ambient fluid, spreading along neutrally buoyant surfaces.

In near-boundary convection, on the other hand, five ingredients are required as suggested by Killworth (1983). First, a ''reservoir'' is required to store dense water. Around Antarctica, wide continental shelves, and in some places topographic depressions, act as salt reservoirs (Gordon 1974; Gordon and Tchernia 1972). The second ingredient is a ''source of dense water,'' which is generally provided by brine release during ice formation (Brennecke 1921). Coastal polynyas, which are mainly produced by offshore katabatic winds, act as a brine factory (Zwally et al. 1985; Cavalieri and Martin 1985) and in some places the intrusion of warm and saline water mass onto the continental shelf plays a role in increasing salinity (Jacobs et al. 1985; Rintoul 1998). Third, a ''dynamic forcing'' is needed to push the dense water out of the reservoir. The onshore advection due to Ekman transport in response to the easterly and katabatic winds along the coast serves to force a return flow at depth out of the continental shelf at a rate on order of about 1 Sv (Sv $\equiv 10^6$ m^3 s^{-1}) (Gill 1973). Fourth, ''more than one water mass'' is involved in the formation of deep and bottom water, that is, on its descent down the continental slope, cold and saline shelf water entrains warmer and saltier Lower Circumpolar Deep Water (LCDW) to finally obtain the properties of AABW (Foster and Carmack 1976). Finally, ''dynamics'' must allow the water to sink since the dense water tends to spread horizontally under geostrophic equilibrium. The thermobaric effect, that is, the pressure dependence of the thermal expansion coefficient, seems to help the dense water mass to sink to great depths (Killworth 1979; Gordon 1998; Akitomo 1999).

The scale of deep convection has been observed to vary with space, time, and convection type. In the case of open-ocean convection, the convective plumes have horizontal scales of 100 to 1000 m, vertical scales of 1000 to 2000 m, vertical velocities of 2 to 10 cm s^{-1}, and timescales from hours to several days (Clarke and Gascard 1983; Rudels et al. 1989; Roach et al. 1993; Schott et al. 1993; Denbo and Skyllingstad 1996; Lab Sea Group 1998; Lilly et al. 1999). Compared to open-ocean convection sites, the scale of near-boundary convection has not been well observed, mainly due to the remoteness and harsh winter conditions. Through a model study, Killworth (1979) implied that a plume associated with the formation of AABW has a horizontal scale on the order of 1000 m, and a vertical velocity of less than 0.5 cm s^{-1}. The vertical scale of near-boundary plumes is estimated to be greater than that resulting from open-ocean convection (Carmack and Killworth 1978; M. Visbeck 1999, personal communication).

Such mesoscale convective events can hardly be resolved in OGCMs, not even with eddy-resolving models. Therefore, this important subgrid-scale ocean phenomenon is still in need of careful parameterization. While a crude parameterization of convection in OGCMs benefits through simplicity and low computational cost, it may have its price by creating poor deep-ocean water mass properties (as pointed out by, e.g., Duffy et al. 1999).

Numerous attempts have been made to improve global-scale ocean properties in OGCMs. Using the Geophysical Fluid Dynamics Laboratory (GFDL) OGCM, Cummins et al. (1990) applied stability-dependent vertical diffusivities and obtained increases in deep-ocean (4000 m) temperature by 0.8°C and salinity by 0.1 psu compared to those achieved with constant diffusivity. Although this measure improved deep-ocean salinity slightly, the global-mean water masses at 4000 m were about 2°C warmer and 1.45 psu fresher than the Levitus climatology suggests. By applying the isopycnal tracer diffusion scheme of Redi (1982) in the GFDL OGCM, England (1993) experienced a remarkably improved representation of Antarctic Intermediate Water (AAIW) and obtained a realistic deep-ocean salinity (34.72 psu vs 34.73 psu at 4000 m), but the deep-ocean temperature remained too low (−0.22°C vs 1.08°C at 4000 m). When Hirst and Cai (1994) increased vertical diffusivity with depth and enhanced isopycnal mixing in presence of horizontal diffusion, the deep-ocean temperature and salinity became much improved, but were still lower than observed by 0.4°C and 0.05 psu, respectively.

In the framework of similar OGCM versions as used by England (1993), the effect of the Gent and McWilliams (1990) parameterization (GM parameterization) has been investigated (e.g., Danabasoglu and McWilliams 1995; Hirst and McDougall 1996; Duffy et al. 1997). In addition to isopycnal tracer diffusion, this scheme features an eddy-induced isopycnal tracer advection. While results with horizontal mixing generally reveal excessive open-ocean convection and largely overestimated deep-ocean temperature (by 1°–2°C) and underestimated deep-ocean salinity (by about 0.2–0.3 psu), convection was drastically reduced, and ocean properties, especially those of AAIW, significantly improved upon introducing the GM parameterization. However, while enhancing the deep-ocean density, the GM scheme tended to decrease the deep-ocean temperature too much by about 0.5°–1°C and the deep ocean remained fresher by about 0.15–0.2 psu than Levitus (1982). Large et al. (1997) obtained overall better deep-ocean properties by using bulk formula to describe the surface heat budget and a more realistic vertical boundary-layer mixing, together with GM parameterization, but a cold and fresh bias of 0.5°C and 0.05 psu was still present below 3000 m. The improved deep-

ocean properties obtained in this simulation, however, are in part due to strong salinity restoring under sea ice.

Investigating the effect of sea ice on long-term deep-ocean properties using a coarse-resolution version of the Hamburg Ocean Primitive Equation (HOPE) model (Drijfhout et al. 1996), which is coupled to a comprehensive sea ice model, Stössel et al. (1998, hereafter SKD) yielded deep-ocean water masses colder by about 0.65°C and fresher by about 0.1 psu than the Levitus climatology. Kim and Stössel (1998, hereafter KS) identified some specific sources influencing the SO water mass properties and obtained improved water masses on and off the Antarctic continental shelves by applying more realistic wind forcing over the SO sea ice and by modifying the model's shelf topography. However, the global-scale deep-ocean water masses remained too cold and too fresh.

These model results have shown that, in general, the simulated deep ocean is colder and fresher than observed. Duffy et al. (1997) pointed out that, although the GM parameterization helps prevent the thermocline from being too diffuse, the deep ocean remains too cold, partially due to too weak NADW penetration to the deep ocean and lower latitudes associated with a weak NADW formation rate by remarkably reduced convection. This has also been stated in England and Rahmstorf (1999). On the other hand, in SKD and KS, the NADW outflow at 30°S appears to be rather realistic (about 17 Sv) and deep, reaching up to 3200 m. In their simulations, the deep-ocean discrepancies are mainly due to excessive open-ocean convection in the SO. This leads ultimately to an insufficient representation of the southward extension of LCDW in the sense of approaching the Antarctic continental margin close enough to realistically contribute to the water mass characteristics of AABW (Toggweiler and Samuels 1995; Duffy and Caldeira 1997; Nakata and Suginohara 1998; KS).

Concerning the possible role of sea ice in modifying the deep-ocean properties, Duffy and Caldeira (1997) suggested distributing released brine due to sea ice formation instantaneously over the upper model layers. This ad hoc measure has been used in several other sea ice–ocean model applications (Maier-Reimer et al. 1993; Pierce et al. 1996; Legutke et al. 1997). In particular, using a GFDL OGCM version coupled to the comprehensive sea ice model of Oberhuber (1993) and employing the GM parameterization, Duffy and Caldeira (1997) redistributed released brine uniformly in the upper 160 m of the water column. This resulted in substantially increased deep-ocean salinity from less than 34.4 psu to close to 34.8 psu. After coupling this sea ice–ocean model to an energy–moisture balance atmosphere model, Duffy et al. (1999) tested the effect of the GM parameterization together with a more physical stability-dependent mixing of rejected salt from freezing (which they refer to as ''plume'' simulation) on global deep-ocean properties. Both applications together led to a substantial improvement of the zonal mean AAIW tongue and deep-ocean temperature and salinity were increased compared to their experiment with GM only. However, deep-ocean water masses remained colder and became saltier than observed. These results suggest that isopycnal diffusion and eddy-induced advection largely contribute to a better reproduction of AAIW and help improve the deep-ocean properties by inhibiting excessive convection. The GM parameterization does not, however, seem to constitute a general recipe for improving deep-ocean water mass properties, as is implied from the experiments of Duffy and Caldeira (1997) and Duffy et al. (1999), and as will be discussed later.

The objective of this study is to investigate and improve the global-scale deep-ocean thermohaline properties and circulation in the framework of a coarse-resolution ocean climate model. The hypothesis behind this objective is that open-ocean convection in the SO is the most critical process in determining these properties, as suggested by others (see above). Our approach is to apply a more physical convection parameterization. We thereby anticipate avoiding direct mixing of relatively fresh and cold Antarctic Surface Water (AASW) down to the deep ocean, which appears to be the main reason for our previous deep-ocean biases (SKD; KS). By weakening the strength of open-ocean convection in the SO, we expect LCDW to extend farther south and to contribute to AABW as a source water together with shelf water. To tackle this problem, we first approach it in an ad hoc manner by simply reducing the frequency of convective adjustment. In the second step, we represent convection in a more physical manner by employing the subgrid-scale plume convection scheme developed by Paluszkiewicz and Romea (1997), which is designed to remove vertical instabilities on scales close to the actually observed convection scale. An alternative method for reducing open-ocean convection in the SO would be the usage of the GM parameterization discussed above. While this would remove the flaw in our model of spurious diapycnal mixing, it seems to have other disadvantages, as indicated above and discussed in section 4.

In the following section, we describe the essentials of the ocean–sea ice model employed in this study, together with the configuration we used and some justification for it. This is followed by a brief description of the new convection scheme, which replaced the original convective adjustment scheme, and the experiments performed in this study. In section 3, the outcome of the experiments obtained with the different convection schemes will be described and discussed. Finally, summary with a discussion as well as a concluding remark follow in sections 4 and 5.

2. Numerical model and experiments

a. Model configuration

This study employs the HOPE OGCM, which is based on the primitive equations with a prognostic free surface

and conservation equations for tracers. It employs the hydrostatic and Boussinesq approximations. The model version used in this study is global with an effective horizontal resolution of 3.5°. It has 11 vertical layers, the finest resolution being the upper layer with 50 m. The time step is 20 hours. The model includes ''real'' bottom topography. The equations are discretized on an Arakawa E grid (Arakawa and Lamb 1977), that is, the model grid consists of two C grids staggered to one another. Detailed features of the ocean model are found in Wolff et al. (1997).

The model includes a comprehensive dynamic–thermodynamic sea ice model (Stössel and Owens 1992). The sea ice dynamics employ the viscous–plastic constitutive law of Hibler (1979) to describe the internal ice stress, while the sea ice thermodynamics are adopted from Owens and Lemke (1990) (see SKD). Because the presence of sea ice influences the air–ice–sea interaction by modifying the albedo, the heat exchange (insulation), and the momentum transfer, the surface heat budget is calculated separately over the ice-free and ice-covered part of a model grid cell. This is to account for the spatially highly differential heat fluxes (Parkinson and Washington 1979).

Overall, the ocean is forced by climatological monthly mean winds from Hellerman and Rosenstein (1983). Based on the positive experience of KS, however, daily European Center for Medium-Range Weather Forecasts winds have been used over SO sea ice. Besides providing a better climatology, the higher wind variability increases the lead fraction and the turbulent heat fluxes, thus enhancing the ice growth rates (SKD). Employing a sea ice–ocean mixed layer model, Stössel (1992) also experienced a substantial enhancement and improvement of the net freezing rate and the oceanic (entrainment) heat flux by using daily instead of monthly winds. Following KS, the present model configuration also includes a widened shelf topography (see section 1).

Potential temperature θ and salinity S are prognostically determined by continuity equations including advection and diffusion (tracer equations). The model does not include isopycnal mixing. In tracer equations, the horizontal diffusity parameter is 2000 $m^2\ s^{-1}$ and the vertical diffusity is $0.5 \times 10^{-4}\ m^2\ s^{-1}$. The treatment of surface temperature and salinity is dependent on the presence of sea ice. In ice-free grid cells, surface temperature and salinity are ''relaxed'' to prescribed air temperature from the Comprehensive Ocean–Atmosphere Data Set (Woodruff et al. 1987) and salinity from Levitus (1982) with timescales of 80 days and 40 days, respectively. As long as grid cells contain sea ice, the surface temperature is assumed to be at the freezing point, nonzero heat fluxes thus giving rise to a change in ice thickness (and compactness), while the surface salinity is modified by the rate of change of ice thickness (Stössel and Owens 1992).

b. Model justification

Under the chosen coarse resolution ($3.5° \times 3.5° \times$ 11 layers), important subgrid-scale processes will need to be parameterized. Ideally, higher-resolution models will reproduce smaller-scale features such as eddies and convection cells. Existing computer capacities, however, do not yet allow eddy-resolving global ocean models (e.g., Semtner and Chervin 1992; Stammer et al. 1996) to be integrated long enough for the deep ocean to reach a near-equilibrium state. In order to learn about the long-term sensitivity of the deep ocean to various processes, the only present-day feasible type of model is thus a coarse-resolution GCM, the kind of which has been widely used for climate studies until recently (Cummins et al. 1990; England 1993; Maier-Reimer et al. 1993; Hirst and Cai 1994; Danabasoglu and McWilliams 1995; Toggweiler and Samuels 1995; Drijfhout et al. 1996; Hu 1997; Large et al. 1997; Duffy and Caldeira 1997; Goosse 1997; etc.). Moreover, long-term global coupled atmosphere–ocean climate modeling studies are still solely accomplished with coarse-resolution (non-eddy-resolving) ocean components (e.g., Delworth et al. 1993; Manabe and Stouffer 1996; Washington and Meehl 1996; Doney et al. 1998; Weatherly et al. 1998; Legutke and Voss 1999; Flato et al. 2000).

The HOPE model includes a detailed sea ice component. This makes it possible to represent the polar surface processes fairly well and more realistically than most other OGCMs. Surface salinity in southern high latitudes was artificially increased to improve the deep and bottom water properties in OGCMs without a sea ice component (e.g., England 1993). While mimicking the first-order effect of brine release, such measures are not sufficient to describe other important features of the ice pack, such as nonlinear interactions between ice dynamics and ice thermodynamics, which has a large impact on the net freezing rate and thus brine release.

c. Convection schemes

Two types of convection schemes are involved in this study. One is the conventional type of vertical mixing over a whole model grid cell in case of unstable stratification (e.g., Wolff et al. 1997). The other is the subgrid-scale plume convection scheme of Paluszkiewicz and Romea (1997).

With the conventional convective adjustment scheme, the stability of each water column is checked every time step by comparing densities between vertically adjacent layers. Density is calculated using the UNESCO equation of state with the updated potential temperature and salinity. If instability occurs, convective adjustment is performed by mixing of each pair of overlying unstable grid layers, that is, for unstable water cells, temperature and salinity are updated based on volume average:

$$\theta_{k-1} = \theta_k = \frac{d_{k-1}\theta_{k-1} + d_k\theta_k}{d_{k-1} + d_k}, \quad (1)$$

$$S_{k-1} = S_k = \frac{d_{k-1}S_{k-1} + d_kS_k}{d_{k-1} + d_k}, \quad (2)$$

where d_k are layer depths for each layer, and k increases with depth. The surface elevation and ice draft is accounted for in d_1. For stable stratification, θ and S remain unchanged.

Having a much more physical justification, the second type of convection scheme is derived from the cumulus convection parameterization used in atmosphere models. As with the conventional convection scheme, the stability of a grid column is checked first. If

$$\rho_{k-1} - \rho_k - \Delta\rho > 0, \quad (3)$$

then the water column is unstable and the model starts mixing. In Eq. (3), $\Delta\rho$ is a stability threshold associated with the inhibiting effects of viscosity and rotation, which retards the initiation of convection. If this threshold is passed, the plume mass flux is calculated following Turner's (1973) entrainment hypothesis:

$$M = b^2 w_p \rho_p, \quad (4)$$

where b is the plume radius, w_p is the downward plume velocity, and ρ_p the plume density. In the first model layer, the plume radius and plume velocity are specified. Next, the vertical variation of mass and momentum flux due to buoyancy forces is calculated for the plume:

$$\frac{dM}{dz} = 2\alpha w_p b \rho_e, \quad (5)$$

$$\frac{d}{dz}(Mw_p) = gb^2(\rho_p - \rho_e), \quad (6)$$

where α is the proportionality coefficient, which is 0.1 following Turner (1973). The variations of subgrid-scale plume temperature and salinity with depth are calculated:

$$\frac{d\theta_p}{dz} = (\theta_e - \theta_p)\frac{1}{M}\frac{dM}{dz}, \quad (7)$$

$$\frac{dS_p}{dz} = (S_e - S_p)\frac{1}{M}\frac{dM}{dz}. \quad (8)$$

Equations (7) and (8) represent the changes in potential temperature and salinity of a fluid parcel with mass flux M descending adiabatically while entraining mass at a rate of dM/dz.

This subgrid-scale water body (plume) penetrates to a neutrally buoyant layer depending on the rate of buoyancy loss at the surface. The final grid-cell-wide potential temperature and salinity are calculated by mixing the plume water properties horizontally with the ambient water masses in each layer based on the volume-weighted average; that is,

$$\Phi = (1 - \sigma_p)\phi_e + \sigma_p\phi_p, \quad (9)$$

where Φ represents the grid-volume-averaged dependent variable; ϕ_e and ϕ_p are the dependent variables in the environment and inside the plumes, respectively; and σ_p represents the fractional coverage of active plumes within a grid cell.

We employ the original parameters of the plume convection scheme, that is, a plume radius of 500 m and a plume vertical velocity in the first layer of 0.03 m s^{-1}, and an entrainment rate of -0.05, together with a stability threshold of -1×10^{-4} kg m^{-3}. Further details of this parameterization can be found in Paluszkiewicz and Romea (1997).

d. Experiments

Four model runs are performed in this study. The first experiment, referred to as REF, features the conventional type of convective adjustment everywhere. In the second experiment, named SCN, the strength of convection is slowed down in the SO by allowing the conventional convective adjustment every 12 model time steps (10 days) rather than every time step. In the third experiment, called MIX, plume convection is applied in the SO, while the conventional scheme is applied in the Northern Hemisphere (NH). In the final experiment, referred to as PCN, plume convection is applied everywhere.

After modifying the convective adjustment and implementing the new convection scheme, we ran another 1000 to 2000 years to obtain near-equilibrium results. Throughout this study, England's (1993) criteria for near-equilibrium were adopted, that is, with a remaining climate drift in global mean temperature and salinity at all model layers of less than 0.01°C/hyr and less than 0.001 psu/hyr, respectively (hyr = hectoyear). Note that since PCN involves a change of the whole conveyor-belt circulation, a near-equilibrium state is not yet reached after 3000 years of integration.

3. Results

In this section, a detailed comparison of the results obtained with the conventional convection scheme (REF and SCN) and those with the plume convection scheme as applied to the SO (MIX) are presented. First, we examine how much the rate of convection has altered with the modified convective adjustment and the new convection scheme. Since the global overturning circulation does not reach the quasi-steady state in PCN, only the change in the rate of convection, which we believe will not be severely affected by the remaining climate drift, is included in the description. Next, we describe the strength of the meridional overturning circulation and associated mass transports. Third, the distributions and properties of the global-scale potential temperature and salinity are described. Then, the meridional heat transport in the global and Atlantic Ocean is illustrated, since it reflects a critical constituent of the

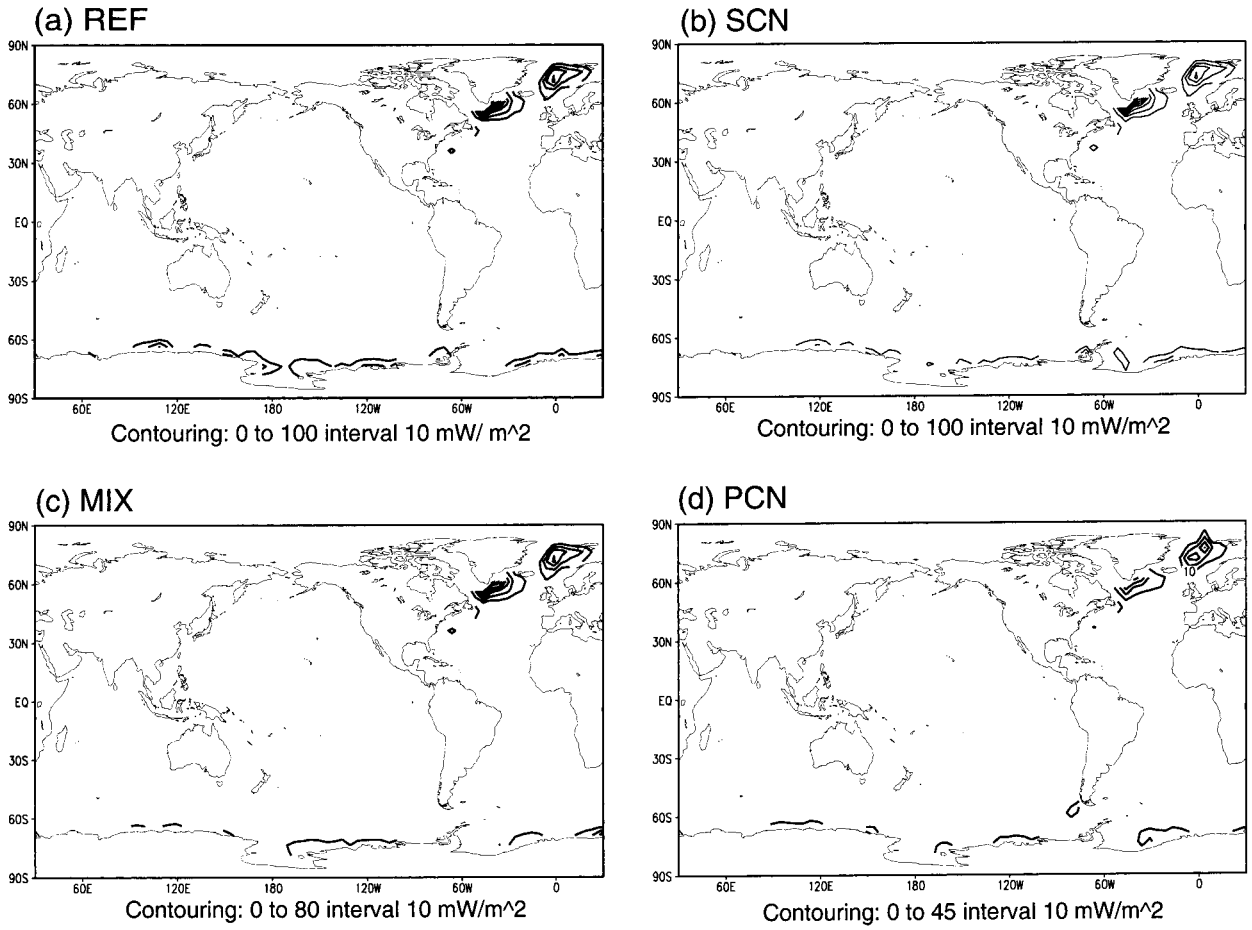

FIG. 1. Annual-mean potential energy release associated with convection simulated in (a) REF, (b) SCN, (c) MIX, and (d) PCN.

global climate system. Finally, the response of SO sea ice distribution and thickness to the treatment of convection is presented.

a. Convection

To measure the strength of convection, we calculated the rate of released potential energy within the water column. Figure 1 shows the areal distribution of annual-mean potential energy release simulated in REF, SCN, MIX, and PCN. In REF (Fig. 1a), the active convection mainly occurs in the Greenland Sea and the Labrador Sea, and most areas around Antarctica. In the NH, the simulated convection regions appear to be generally coincident with observations (see Marshall and Schott 1999), but in the SO they are more abundant than observations indicate, especially in the eastern Pacific sector (80°–160°W) and the eastern part of the Weddell Sea (10°W–30°E) where convection is observed to be less active (Killworth 1983).

Reducing the convection frequency from 20 h to every 10 days (SCN) decreases convection significantly around Antarctica (Fig. 1b), but remains too strong in the Pacific sector and east of the Weddell Sea. With the plume convection scheme (MIX and PCN), the rate of convection decreases further in the SO, in general agreement to what has been inferred from observations (Figs. 1c and 1d). As expected, in PCN, the rate of convection also decreases substantially in the NH. It is notable, however, that in spite of this decrease, deep-penetrating open-ocean convection is still well maintained in the GIN Sea and the Labrador Sea, while it pretty much vanished in the Southern Hemisphere (SH). This is consistent with observations (e.g., Marshall and Schott 1999, and references therein) and emphasizes the importance of a more physical and subgrid-scale treatment of open-ocean convection to capture these hemispheric differences in global OGCMs.

The seasonal variation of convection averaged from 40° to 90° in both hemispheres is shown in Fig. 2. Featuring a strong seasonal cycle, the maximum convection occurs in August in the SH and in February in the NH in REF. The maximum SH convection decreased by about 30% in all sensitivity experiments, while in the NH convection slightly increased in SCN and MIX, but significantly decreased in PCN. The SH maxima are

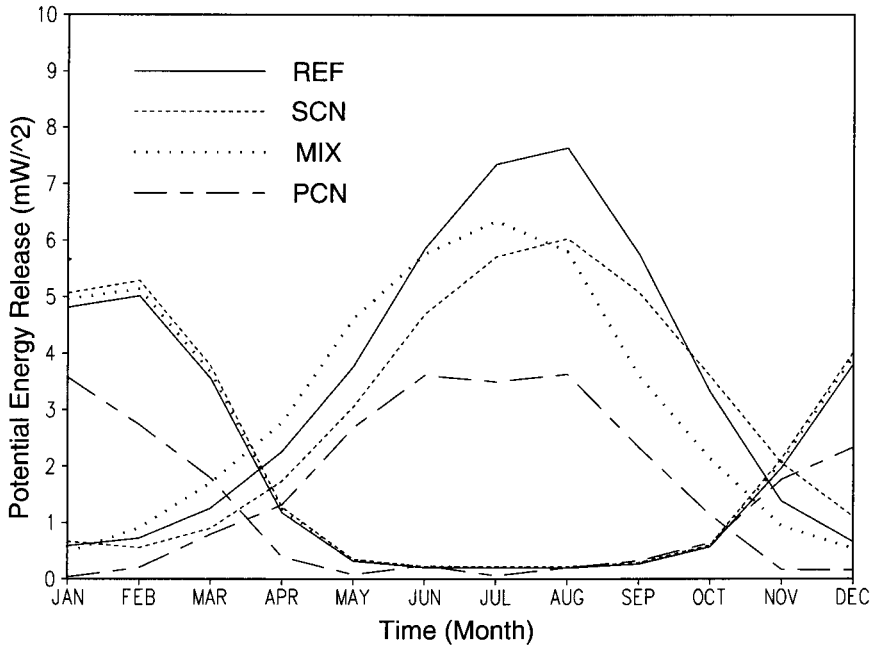

FIG. 2. Seasonal cycle of hemispherically averaged potential energy release due to convection of experiments REF (full line), SCN (short-dashed line), MIX (dotted line), and PCN (long-dashed line).

encountered roughly one month earlier when the plume convection scheme is applied (Fig. 2). This seems to be associated with the sensitivity of the two different types of convection schemes to the change in surface forcing. With the plume convection scheme, convection can be initiated on a small horizontal scale, thus requiring a relatively small change in the buoyancy forcing for convection to occur. With conventional convective adjustment, on the other hand, an order 100-km grid cell needs to be rendered unstable for convection to be initiated.

Using the GFDL OGCM, Danabasoglu and McWilliams (1995) and Hirst and McDougall (1996) also obtained excessive convection, which they attributed to spurious diapycnal mixing resulting from horizontal mixing across isopycnals. They effectively reduced convection by introducing the isopycnal tracer advection scheme of GM (see section 1). The result in PCN in terms of the areal distribution of convection is comparable to that obtained by Danabasoglu and McWilliams (1995). The strength of convection, however, seems to be much larger (two to three orders of magnitude), as indicated in Duffy et al. (1997), who used a similar model setup. In particular, their simulation with horizontal and stability-dependent vertical mixing (run 3: their Fig. 1) reveals very similar magnitudes as in our PCN case. As pointed out by Danabasoglu and McWilliams (1995), diapycnal mixing is dramatically reduced upon introducing the GM parameterization. For the same reason, the GM parameterization also results in a remarkable decrease of convective potential energy release to effectively zero (Duffy et al. 1999). In our case, on the other hand, while the plume scheme reduces overall convection, it still allows for open-ocean convection in the GIN Sea and (near-boundary) convection along Antarctica. The latter is required to produce AABW (Foster and Carmack 1976; Carmack and Killworth 1978), ideally as a product of high salinity shelf water and modified Circumpolar Deep Water (CDW).

b. Meridional overturning and mass transport

Figure 3 shows the zonally integrated global and Atlantic meridional overturning streamfunction. The maximum strength of the SO cell, mainly associated with regional overturning in the Weddell and Ross Seas, decreases slightly and becomes narrower in REF than in SKD (Fig. 3a). This is due to the widened shelves in the Weddell and Ross Seas (see section 2). Parts of AABW produced near the Antarctic continental margin flow northward along the western boundary across the equator, constituting the SH cell. In REF, the SH cell appears to be about 15 Sv in the world's ocean basins and about 6 Sv in the Atlantic, which is in good agreement with the observed estimates (~6.9 Sv from Hogg et al. 1999). General discrepancies in observed estimates were discussed in SKD.

In experiment SCN (Fig. 3c), the magnitude of the SO cell decreased slightly by about 0.5 Sv, while its depth remained up to 3000 m. Thus, while convection occurs less frequently, once initiated, it is still deep penetrating. On the other hand, with the plume convection scheme (MIX) (Fig. 3e), the magnitude of the

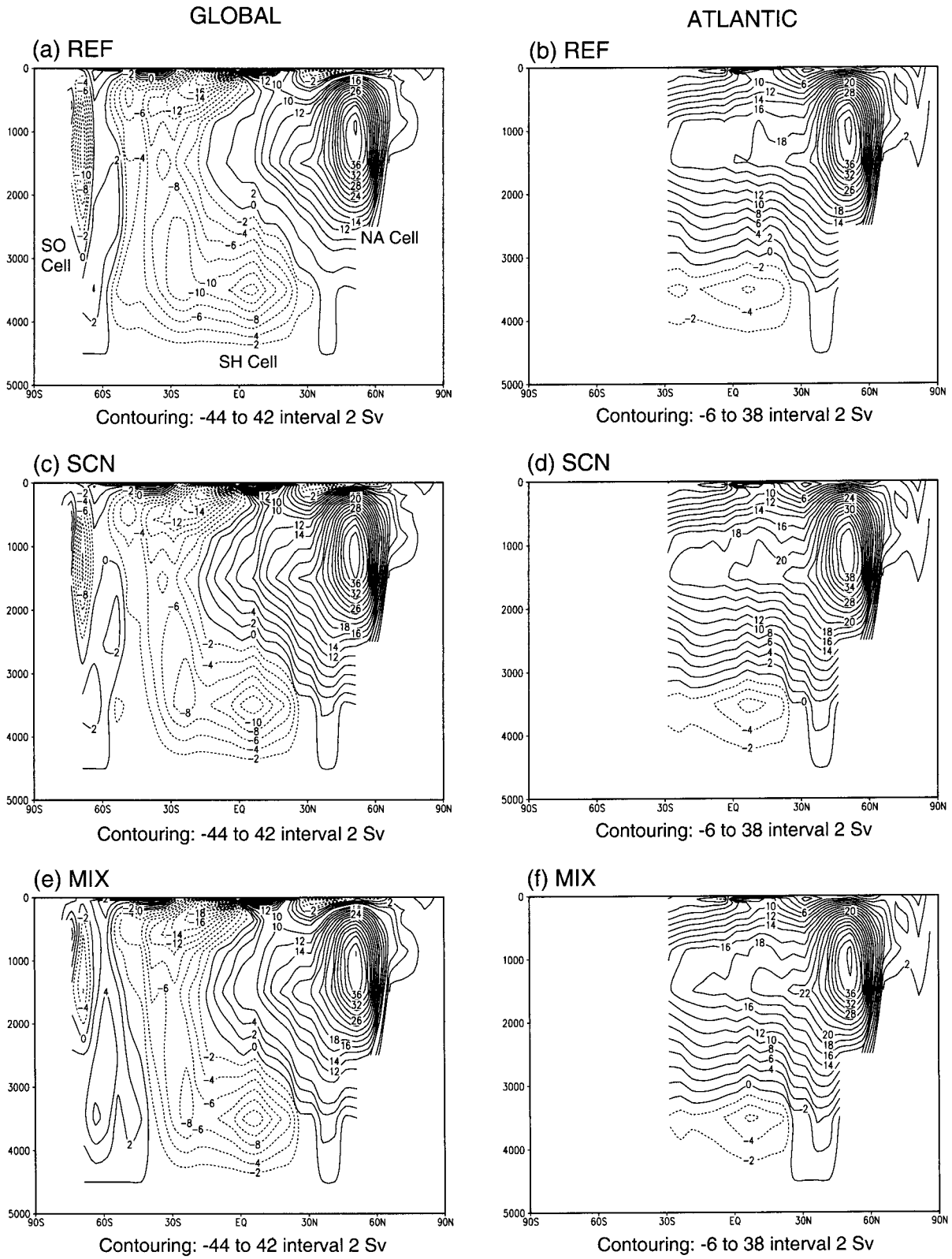

FIG. 3. Annual-mean global and Atlantic meridional overturning circulation of (a) and (b) REF, (c) and (d) SCN, and (e) and (f) MIX.

SO cell decreases substantially by 5.5 Sv. Moreover, the depth of convection becomes far shallower to less than 2000 m, which seems to be a much more realistic feature, for example, for the open-ocean convection scale of the Weddell polynya (Gordon 1978; Gordon and Huber 1990).

The SH cell is decreased by about 1.5 Sv in both SCN and MIX. This suggests that the large-scale effect of a more detailed plume convection in the SO is not different from reducing convection in an ad hoc manner. On the other hand, regional water mass properties, including LCDW, were improved substantially, thus improving the source water properties (e.g., Price and Baringer 1994) for AABW (see next section).

In SCN, the NADW outflow at 30°S increased significantly by about 2 Sv (Fig. 3d), whereas it increased only slightly by about 0.5 Sv in MIX (Fig. 3f). On the other hand, there is no consistent change in the Atlantic part of the SH cell compared to REF. This implies that the NADW outflow is not governed by the change in the rate of AABW production and outflow. Similar results have been found in other model studies (e.g., Stocker et al. 1992; England 1993; Fichefet et al. 1994; Cai and Greatbatch 1995). In all experiments, the AABW intrusion across the equator in the Atlantic basin appears to be about 6 Sv. This figure is well within the uncertainty range of observational estimates.

In REF, the net transport of the Antarctic Circumpolar Current (ACC) through Drake Passage is 109 Sv, which is much closer to observed estimates than those of SKD and Drijfhout et al. (1996). This is mainly due to the consideration of synoptic-scale variability in the wind forcing over SO sea ice, which enhances the freezing rate over more frequently occurring leads, and thus the meridional density gradient. Although the ACC transport is underestimated compared to observed estimates (~130 Sv from Whitworth and Peterson 1985) or inverse modeling products (~140 Sv from Macdonald and Wunsch 1996), it is expected to improve, among others, with a wider Drake Passage (Drijfhout et al. 1996). The simulated Indonesian Throughflow in all experiments is around 20 Sv, which is within the uncertainty range of observational estimates (e.g., 15–20 Sv from Fieux et al. 1994).

In SCN, the ACC transport is decreased by about 7 Sv, whereas in MIX, it decreased substantially by about 20 Sv. This change of the ACC transport is consistent with that of the SO cell because the former is largely determined by the meridional density gradient (e.g., Cai and Baines 1996), which decreases when less AABW is produced.

c. Deep-ocean thermohaline properties

Figure 4 shows observed meridional sections of potential temperature and salinity in the Atlantic Ocean averaged between 10° and 60°W. The data are from Levitus (1982). One of the salient features shown in the meridional sections is the southward extension of the warm and saline tongue associated with NADW and CDW in the SO.

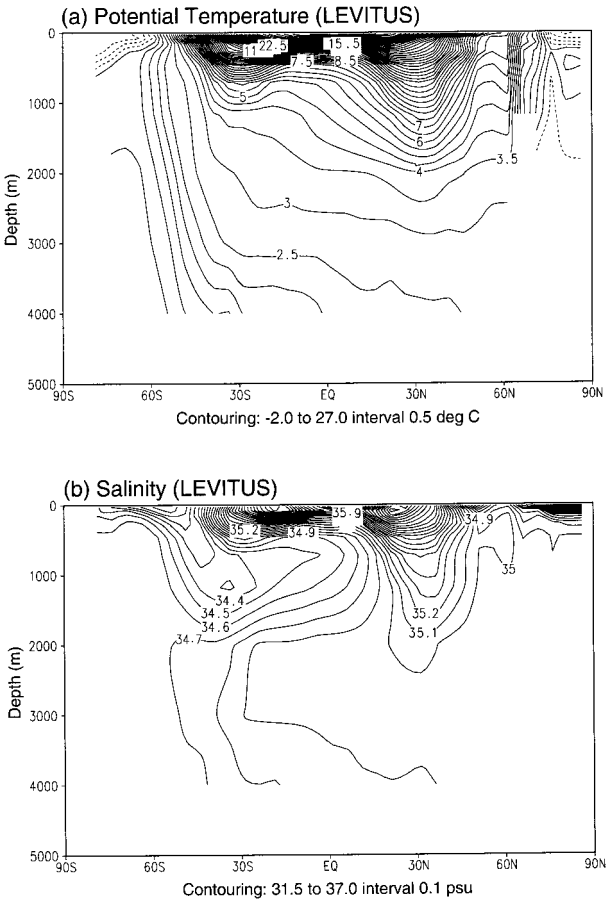

FIG. 4. Annual-mean meridional section of western Atlantic (averaged between 60°W and 10°W) observed (Levitus 1982) (a) potential temperature and (b) salinity.

CDW is composed of two parts. The upper part of CDW, which originates in the Indian and Pacific Oceans (Callahan 1972), is characterized by an oxygen minimum and a temperature maximum. The lower part of CDW (LCDW), on the other hand, reflects properties of NADW and is characterized by a salinity maximum (Whitworth and Nowlin 1987). Produced in the northern North Atlantic, NADW propagates toward the south along the western boundary and joins the ACC in the southwestern Atlantic at about 45°S (Reid and Lynn 1971). In the ACC regime, NADW blends with other water masses of the SO, retaining the properties of LCDW. Flowing toward the east along the ACC, warm and saline LCDW shoals up toward the Antarctic continental margin where it meets colder and usually fresher waters from the Antarctic shelves. The core of maximum potential temperature and salinity of LCDW is found from 150 to 1200 m (about 600 m on average) around Antarctica (Kim 1995). The southward extension of LCDW terminates at the continental slope everywhere

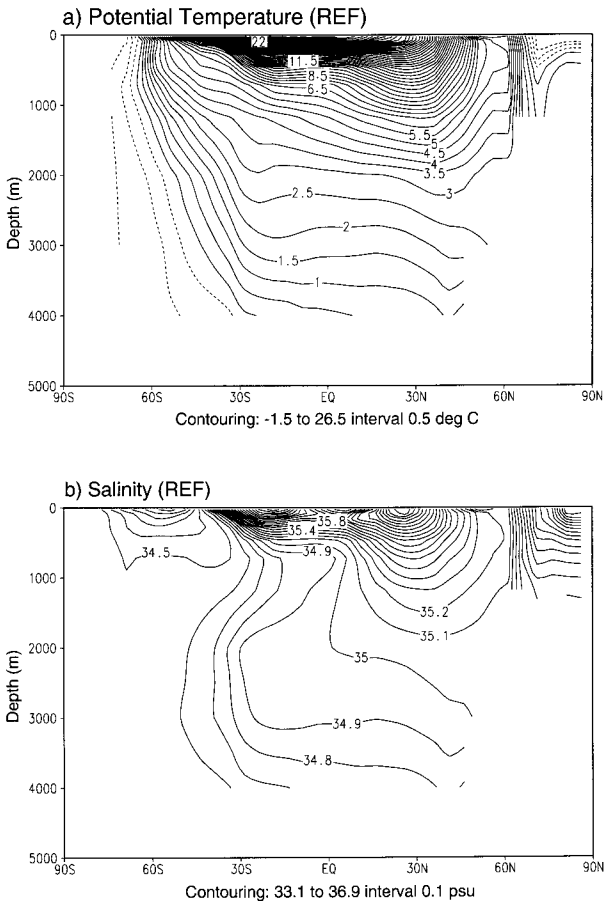

FIG. 5. Annual-mean meridional section of (a) potential temperature and (b) salinity of REF. Otherwise, same as Fig. 4.

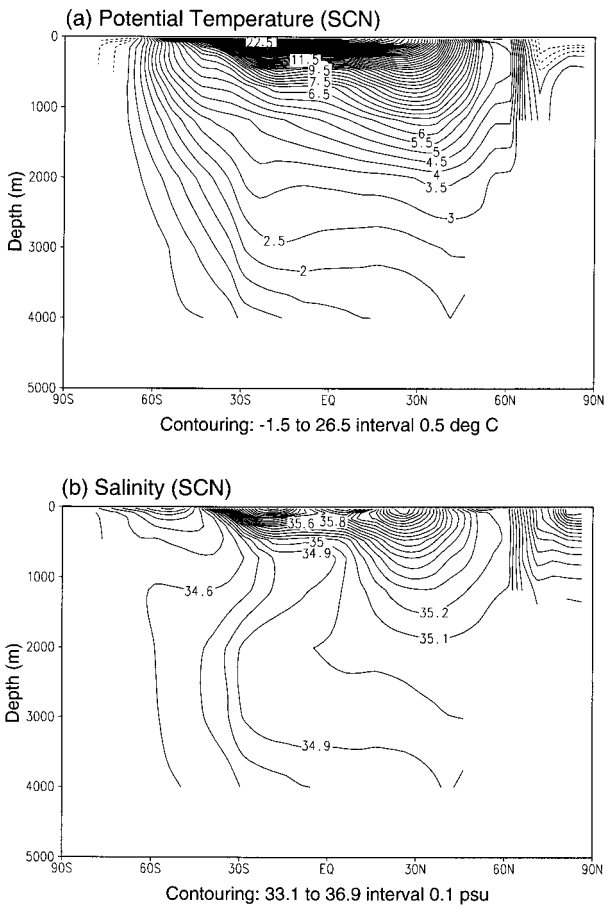

FIG. 6. Annual-mean meridional section of (a) potential temperature and (b) salinity of SCN. Otherwise, same as Fig. 4.

around Antarctica except in the Bellingshausen and Amundsen sector where it continues onto the continental shelf.

The Levitus temperature section shows that the SO intermediate water between 500 and 1500 m has temperature greater than 0°C, characterizing LCDW, and AABW lying below LCDW has temperature less than 0°C. Besides contributing to the formation of AABW (see section 1), LCDW plays a role in maintaining the stability of the SO water column. Therefore, the representation of LCDW properties and its extension toward the south is critical in reproducing the properties of AABW in OGCMs.

Another distinct feature in the observed meridional section of water mass properties is the low salinity AAIW tongue deepening northward to about 1000 m (see Fig. 4b). Different opinions have been reported in terms of the formation mechanism of AAIW and its source water. While McCartney (1977) proposed that AAIW is primarily produced in the southeast Pacific Ocean where subantarctic mode water is transformed into AAIW and flows into the South Atlantic, Molinelli (1981) suggested that it is formed by an isopycnal mixing of AASW with subsurface waters in the Antarctic Polar Front regions. Whatever the production mechanisms, the isopycnal mixing seems to be critical in transferring the low salinity AASW northward to eventually constitute and maintain the AAIW tongue.

Figure 5 presents the simulated meridional sections of potential temperature and salinity with the conventional convection scheme (REF). As mentioned in section 1, the simulated temperature is overall much colder than observed, especially in the SH and below 2000 m (Fig. 5a). The 3°C isotherm, for example, is located between 2500 and 3000 m around the equator in the Levitus data (Fig. 6a), whereas it occurs shallower than 2000 m in REF. This trend gets more severe with depth and toward the SO where the whole water column is filled with cold water of temperature less than −1.5°C. Furthermore, the warm tongue of CDW extension toward Antarctica is absent.

Up to about 30°S, the deep-ocean salinity associated with NADW is relatively well reproduced (Fig. 5b), but farther south it becomes fresher than observed and the southward extension of NADW is not that distinct (see Fig. 4b). For example, the observed isohaline of 34.7

TABLE 1. List of globally averaged deep ocean (400 m) potential temperature (θ) and salinity (S), the magnitude of overturning circulation in the Southern Ocean (SO), outflow of AABW across the equator (SH), the transport of the ACC as given by the Drake Passage throughflow, the strength of NADW outflow across 30°S, the mass transport of the Indonesian Throughflow (IT), the northward heat flux (HF) at 30°N in the Atlantic Ocean. OBS is abbreviated for observed estimates, REF for reference experiment, SCN for slow convective adjustment in the SO, and MIX for plume convection in the SH and convective adjustment in the NH. The source of the observed estimates are Levitus (1982) for deep-ocean temperature and salinity, Macdonald and Wunsch (1996) for the SH cell, NADW outflow, and HF, Whitworth and Peterson (1985) for the ACC, and Fieux et al. (1994) for IT.

Exp	θ (°C)	S (psu)	SO (Sv)	SH (Sv)	ACC (Sv)	NADW (Sv)	IT (Sv)	HF (PW)
OBS	1.08	34.73	—	~12	130	~17	15–20	1 (±0.3)
REF	−0.21	34.63	11.5	15.0	108.9	15.2	20.7	0.78
SCN	0.85	34.70	10.0	13.5	102.0	17.7	20.1	0.82
MIX	0.93	34.72	6.0	13.5	89.7	15.7	21.4	0.81

psu penetrates as far south as about 55°S below 2000 m. South of that latitude the salinity is observed to be greater than 34.6 psu. The simulated salinity, however, is less than 34.6 psu south of about 50°S.

In addition to the meridional property sections, the globally averaged deep-ocean potential temperature and salinity at 4000 m are −0.21°C and 34.63 psu (Table 1). These values are far lower than the observed values at that depth (1.08°C and 34.73 psu). A similar, if not much stronger, fresh bias is obtained in many other OGCM studies (see section 1).

This discrepancy has also been noted in KS (see section 1). With widened shelf topography in the Weddell Sea and the Ross Sea to provide a reservoir for salt accumulation, and with daily instead of monthly winds over SO sea ice, both modifications of which are considered in this study, the global-scale world's deep-ocean water mass properties turned out to become even fresher and colder than SKD. The more variable winds tend to increase sea ice formation and consequently enhance brine release over the Antarctic shelf and oceanic regimes. In the shelf regime, increased brine seems to play a desirable role by activating near-boundary convection and providing more salt to the shelf floor. However, in the oceanic regime, the increased brine acts to degrade deep- and bottom-water properties by enhancing the rate of open-ocean convection. On the other hand, variables such as sea ice thickness and water mass profiles on and off the Antarctic shelf were improved under the more realistic boundary conditions (see KS).

The fresh and cold bias of the simulated deep and bottom water seems to be ascribed to two main reasons. First, AASW is predominantly involved in the formation of AABW, as pointed out by Duffy and Caldeira (1997). The characteristics of AABW ($-1.7°C < \theta < 0°C$ and $34.65 < S < 34.73$ psu) are known to be primarily determined by mixing of cold and moderately saline shelf water ($\theta < -1.7°C$ and $S > 34.50$ psu) with warm and saline LCDW ($\theta > 0°C$ and $S > 34.70$ psu) mainly through near-boundary convection and downslope mixing. In the model, however, AABW characteristics are mainly determined by the properties of AASW as a result of strong open-ocean convection. AASW has a temperature close to the freezing point (cold) during the time of active convection and a salinity of usually less than about 34.5 psu (fresh) in the Antarctic oceanic regime (Kim 1995; Whitworth et al. 1998).

Second, the simulated intermediate water mass of the SO is too cold and too fresh due to the lack of LCDW properties. When densified surface water due to cooling and/or brine release mixes down, it is presumed to mix with an underlying warm and saline water mass. However, in the model the underlying intermediate water mass is quite cold ($\theta < 0°C$) and fresh ($34.5 < S < 34.6$ psu) (see Fig. 5), presumably because the southward extension of LCDW is hampered by strong open-ocean convection. Toggweiler and Samuels (1995) argued that the southward extension of LCDW could also be hampered by an inadequate simulation of the ocean's circulation. In either case, this would lead to a too cold and fresh resultant AABW mixture.

The two reasons for the fresh and cold bias of simulated deep and bottom water are interrelated because the problem originates from a common source, that is, too strong open-ocean convection in the SO. Upon modification of the convective adjustment or implementation of plume convection in the SO, deep-ocean temperature and salinity show significant increases toward observed values, mainly as a result of substantially decreased SO convection.

In the potential temperature section of SCN (Fig. 6a), the deep SO water mass attains temperature between −0.5° and 0°C, which is significantly improved over REF. However, the temperature signal of LCDW does not extend far enough to the south. The meridional salinity section of SCN reflects a more realistic southward extension of NADW (Fig. 6b). For example, the 34.6 psu isohaline extends farther south beyond 60°S and to shallower layers than in REF. In response to the advanced southward extension and shallowing of warm and saline LCDW, the low salinity AAIW tongue is more distinct in SCN than in REF, although the salinity minimum remains still too high along the core compared to the observed section (see Fig. 5b). In this experiment, the globally averaged deep-ocean potential temperature and salinity increased substantially to 0.85°C and 34.70 psu, which are far closer to the observed than those of REF (Table 1).

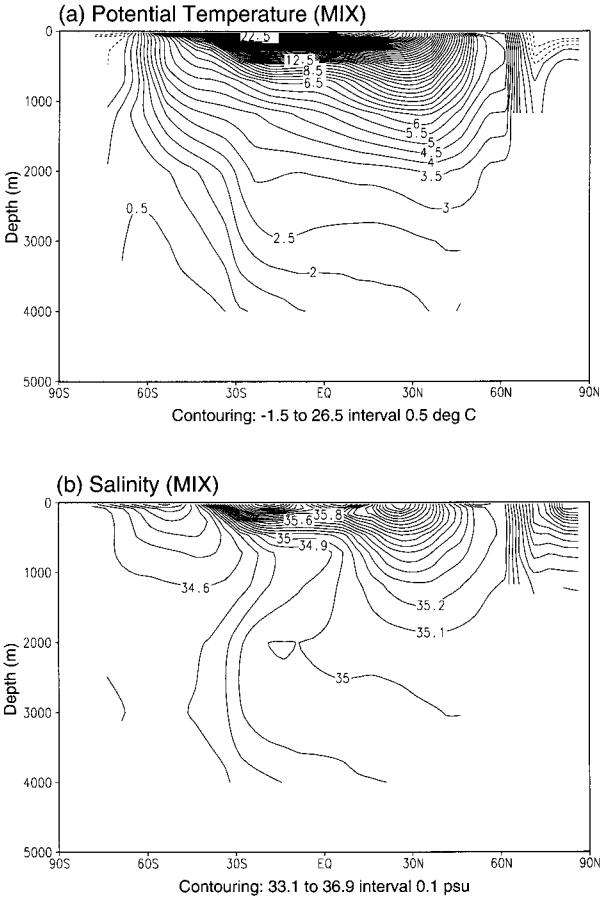

FIG. 7. Annual-mean meridional section of (a) potential temperature and (b) salinity of MIX. Otherwise, same as Fig. 4.

Upon replacing convective adjustment with the plume convection scheme in the SO (MIX) (Fig. 7a), the vertical–meridional structure of the isotherms in the western Atlantic gets even closer to the observed than in SCN. In the deep SO, negative temperature completely disappears and there is a tendency of a warm tongue of LCDW extending up to the Antarctic continental margin. Moreover, the upper-layer water masses of the SO become stratified and the global mean potential temperature at 4000 m yields 0.93°C, which is a further improvement over SCN (0.85°C) toward the observed estimate (1.08°C).

The simulated salinity is also overall improved in MIX. In the SO, salinity ranges between 34.6 and 34.7 psu below about 1000 m (Fig. 7b), which is almost coincident with the observed (see Fig. 5b). The globally averaged deep-ocean salinity (34.72 psu) is within the observed value (34.73 psu). This increased deep-ocean salinity in MIX seems to be related to the slightly increased NADW outflow toward the south. For example, the isohaline of 35.0 psu is extended farther south beyond the equator and slightly deeper than observed (see Fig. 5b).

The increase of the deep-ocean temperature and salinity in SCN and MIX is consistent with changes in the strength of the overturning circulation. In experiment SCN, the SO cell and the SH cell decreased by about 2 Sv, whereas warm and saline NADW outflow at 30°S increased by a comparable amount (see Fig. 3). In contrast, in MIX, only slight changes are detected in the SH cell and in NADW outflow, while the strength of the SO cell decreased substantially by about 5.5 Sv compared to REF. This suggests that in SCN the increased deep-ocean thermohaline properties are attributed to the enhancement of NADW outflow, while the persistently strong and deep SO cell seems to hamper the extension of CDW farther south beyond about 60°S. On the other hand, in MIX, the substantially weakened and shallower SO cell associated with the subgrid-scale and overall shallower convection seems to allow warm and saline LCDW to reach farther to the south, eventually increasing the global deep-ocean potential temperature and salinity very close to observed values.

Vertical profiles of global mean potential temperature and salinity are shown in Fig. 8. At layers shallower than 1000 m, the simulated temperatures in REF are warmer than observed, while they are colder in deeper layers. In SCN and MIX, the deep-ocean temperatures below 1000 m are substantially increased (dotted and dashed lines in Fig. 8a). The potential temperature is almost coincident with the Levitus profile below 2000 m. In terms of the global mean salinity profile, there is a large discrepancy between observation and simulation above 2000 m (Fig. 8b). A distinct salinity minimum is present in the Levitus profile associated with AAIW, which can hardly be traced in the simulated profiles. In deeper layers, however, salinity profiles of SCN and MIX are substantially improved over REF.

With the ad hoc or the more physical convection parameterization in the SO, the representation of AAIW is not improved. This seems to be related to the earlier mentioned problem of spurious diapycnal mixing associated with the usage of horizontal tracer mixing. By employing isopycnal tracer diffusion and advection (GM parameterization), AAIW has been captured much more realistically (Danabasoglu and McWilliams 1995; Duffy and Caldeira 1997; Duffy et al. 1999). In particular, cold and fresh AASW seems to have been readily transferred northward along isopycnal surfaces. The new convection scheme, on the other hand, inhibits a direct influence of AASW on deep-ocean properties and thus results in overall improved deep water masses. Problems resulting from the horizontal mixing scheme seem to be limited to the frontal regions across the ACC, along which AAIW enters deeper layers (see, e.g., Fig. 9 in Hirst and McDougall 1996).

d. Meridional heat fluxes

The oceanic heat transport is a critical component in the global climate system. Because the meridional heat

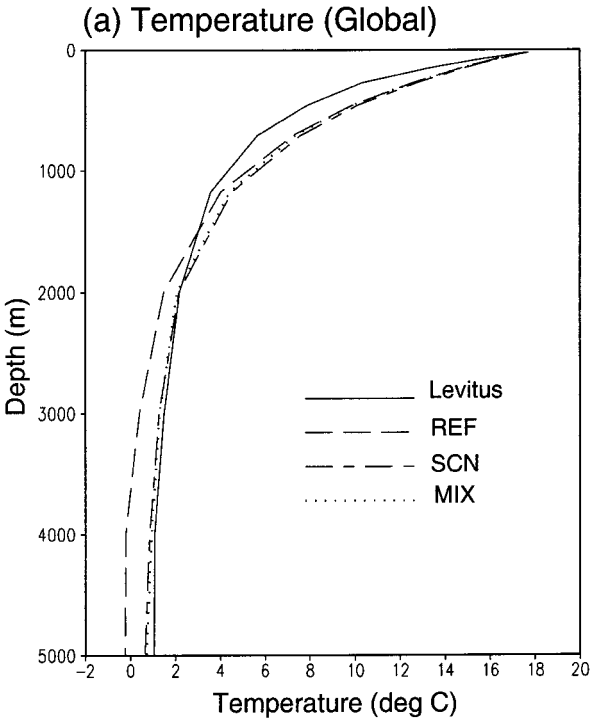

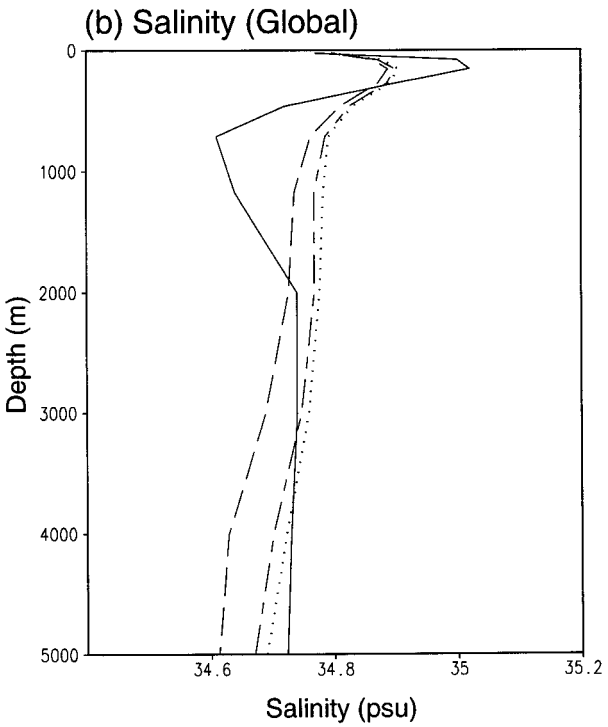

FIG. 8. Vertical profiles of globally averaged (a) potential temperature and (b) salinity as observed (Levitus; full line), and simulated in REF (long-dashed line), SCN (short-dashed line), and MIX (dotted line).

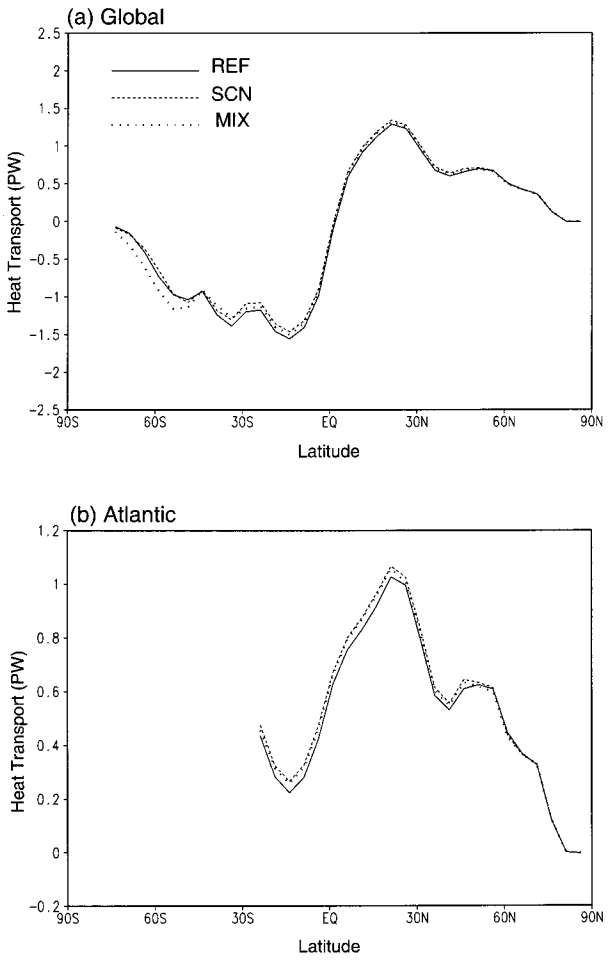

FIG. 9. Zonally integrated annual-mean meridional heat transport for (a) all ocean basins and for (b) the Atlantic basin simulated in REF (full line), SCN (dashed line), and MIX (dotted line).

transport is predominantly determined by the upper-layer temperature and circulation, a large modification of this quantity by changing the convection in the SO is not expected. Nevertheless, a significant modification in the meridional heat transport is registered, though mainly limited to the SO (Fig. 9).

In REF (Fig. 9a), the maximum northward heat transport occurs at around 15°N with over 1.5 PW (PW = 10^{15} W). This figure is within the error range of observed estimates (e.g., Hastenrath 1982; Talley 1984). At 30°S, the maximum simulated southward heat transport is also about 1.5 PW, which seems substantially overestimated over what Macdonald and Wunsch (1996; 0.9 PW) retrieved.

In the Atlantic Ocean north of 30°S, the meridional heat transport is northward everywhere (Fig. 9b). This is due to the northward mass transport in the upper layer (thermocline) of the Atlantic Ocean, referred to as the warm water route (Gordon 1986). As mentioned in the previous section, warm NADW enters the ACC regime where it upwells into shallower layers. Flowing toward

the east with the ACC, some portion of the upwelled NADW recirculates to the Indian and Pacific Oceans. From there, it flows into the Atlantic Ocean with the Agulhas Current, subsequently flowing northward in the subtropical gyre of the South Atlantic.

By limiting convection in SCN, the SO meridional heat transport is hardly altered, while with plume convection (MIX) it increases substantially by about 30% (Fig. 9a). This enhancement is consistent with shallower and weaker SO open-ocean convection allowing for a more vigorous southward extension of LCDW. The simulated heat transport in the Atlantic Ocean appears to be overall underestimated, especially in the Tropics (Fig. 9b). With reduced SO convection in both SCN and MIX, the northward heat transport in the Atlantic is overall increased, especially in SCN. This increase seems to be driven by the increased NADW outflow (Fig. 3d), which ultimately increases the warm upper-layer return flow to the north.

e. Sea ice

In the SO, the production of new ice is an important constituent in producing dense water (Zwally et al. 1985; Cavalieri and Martin 1985). Therefore, a reasonable simulation of sea ice processes in OGCMs is a crucial issue, for example, for the formation of AABW. Convection influences the vertical oceanic heat flux, which in turn modifies sea ice. In this section, we describe the associated changes in sea ice.

Gloersen et al. (1992) provided monthly sea ice concentration retrieved from satellite passive-microwave sensors for 10 years from 1978 to 1987. The 10-yr averaged SO wintertime sea ice distribution is summarized as follows. Defining the ice edge at 15% ice concentration, the maximum sea ice extent reaches equatorward to 55°S in the Weddell Sea from 60°W to 20°E and then rapidly retreats poleward to 60°S to about 70°E. It further retreats close to the continent at about 135°E. In the Ross Sea, sea ice extends again equatorward to 60°S, specifically in the eastern part, shrinking to 65°S toward the Bellingshausen and Amundsen Seas (70° and 130°W).

The distribution of the Antarctic sea ice in winter is somewhat correlated with the location of the southern boundary of the ACC, commensurate with the southernmost extension of the upper part of CDW (Orsi et al. 1995). At the western limbs of the extensive cyclonic gyres of the Weddell Sea and the Ross Sea, the southern boundary of the ACC is located farther north than elsewhere, which is reflected in a relatively large sea ice extent. The wintertime SO ice thickness is observed to be mostly around 0.5 m, while in the presence of ridging the average ice thickness may reach up to 2.5 m (Wadhams 1994; Worby et al. 1996).

Figure 10 shows the simulated SO mean sea ice thickness for August. The ice edge is defined at 0.1 m. Although sea ice thickness is improved with more variable

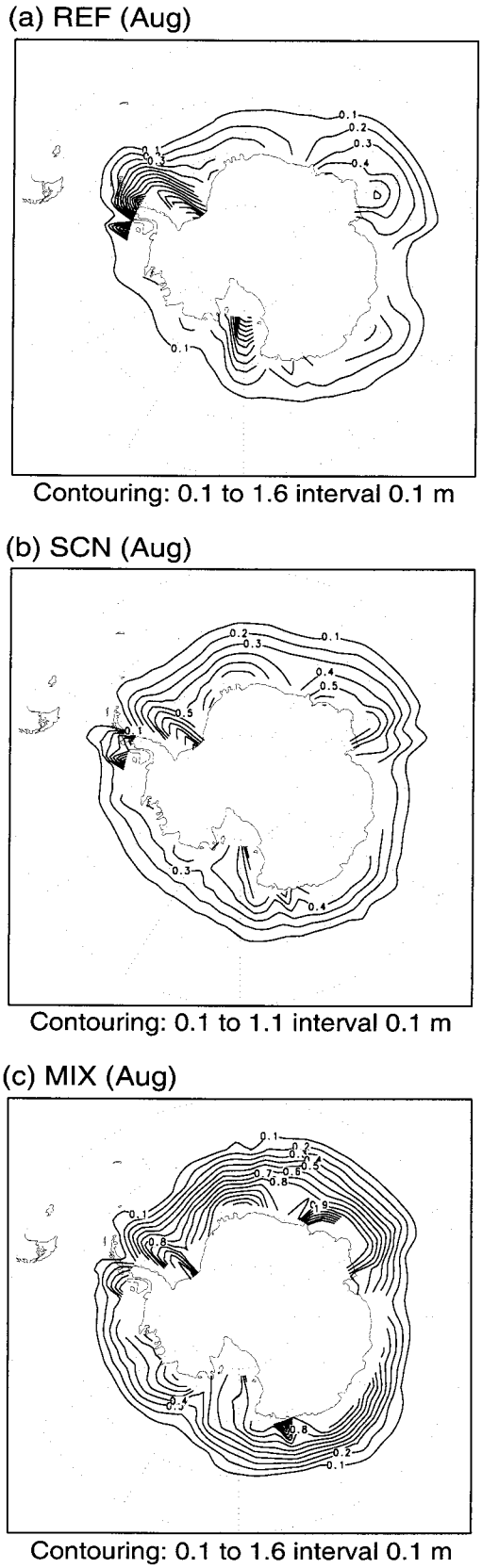

FIG. 10. Winter ice-thickness distribution in the Southern Hemisphere as simulated in (a) REF, (b) SCN, and (c) MIX.

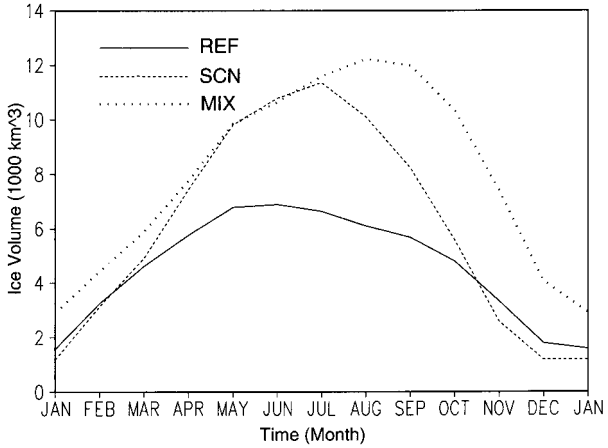

FIG. 11. Seasonal cycle of Antarctic ice volume simulated in REF (full line), SCN (dashed line), and MIX (dotted line).

winds and widened shelf topography (see KS), it is still substantially underestimated in REF (Fig. 10a). Excessive upward oceanic heat flux associated with excessive open-ocean convection seemed to be a plausible reason for this (Martinson 1990). Indeed, with reduced convection in SCN, the sea ice extent and thickness increased substantially over wide portions of the SO. Duffy et al. (1999) also obtained an increased sea ice area by weakening SO convection, either by introducing GM parameterization and/or instantaneously distributing rejected brine over the upper water column.

In MIX, the SO sea ice thickness increases even more to an average of about 0.5 m, which is in fairly close agreement to what is observed. Moreover, the sea ice extent is more realistic everywhere around Antarctica, except for the northward extension in the Weddell Sea and the Ross Sea. The overall improvement in sea ice distribution and thickness in MIX versus SCN seems to be clearly related to the more physical treatment of convection with the plume scheme leading to a major upgrade of the regional subsurface water mass properties, in particular LCDW, and thus also of the vertical entrainment heat flux.

The SO ice extent is observed to vary from about 4 $\times$ 10^6 km^2 in January to around 19 $\times$ 10^6 km^2 in September (Gloersen et al. 1992; Weatherly et al. 1997). With an average ice thickness of about 0.5 m, the ice volume varies seasonally approximately between 2 $\times$ 10^3 km^3 and 9.5 $\times$ 10^3 km^3 for the same months. Figure 11 shows the simulated SO seasonal ice volume. In REF, the seasonal cycle of ice volume, as well as its annual average, are substantially underestimated with an annual mean 4.7 $\times$ 10^3 km^3, and the maximum appears several months earlier than observed. In SCN, the seasonal amplitude as well as the average ice volume increased substantially up to 6.3 $\times$ 10^3 km^3, fairly close to what can be retrieved from observations. The winter maximum, however, still appears earlier than observed by two months. The SO ice volume increases further in MIX to an average value of about 8.3 $\times$ 10^3 km^3, which is in reasonable agreement with observations. Moreover, the simulated seasonal cycle is now in phase with the observed one (e.g., Gloersen et al. 1992). This phase shift in *ice volume* toward the *later* part of the season upon switching to plume convection (MIX) is consistent to the phase shift of *convection* toward the *earlier* part of the season in MIX (and PCN) (Fig. 2). The earlier initiation of convection with the plume scheme enhances upward oceanic heat flux, which in turn retards ice formation in the fall season. The more detailed plume convection thus seems to rectify the timing for tapping of warmer water masses (in this case LCDW) from underneath, which is not captured with the conventional convective adjustment scheme.

4. Discussion

This paper aimed at investigating and improving the global-scale deep-ocean thermohaline properties that have chronically appeared to be colder and fresher than observed in most OGCMs [as pointed out by, e.g., Duffy and Caldeira (1997)]. An improvement of the SO regional water masses was attempted in KS by applying more realistic wind forcing over SO sea ice together with a widened and more realistic shelf topography. While regional features were improved, the more realistic wind forcing actually degraded the global-scale deep-ocean thermohaline properties. This was caused by enhanced open-ocean convection in the SO due to increased sea ice formation and brine release with the more variable winds. The excessiveness of open-ocean convection was attributed to an oversimplified parameterization of vertical mixing to remove instabilities, involving quasi-instantaneous vertical overturning of an order 100 km horizontal grid scale, about two orders of magnitude larger than the observed convection scale.

While one key to the problem of excessive open-ocean convection is the crude convective adjustment parameterization, another one is spurious diapycnal mixing associated with horizontal tracer diffusion, particularly across steep-sloping isopycnal surfaces. This problem has been realized in many recent studies (e.g., Gent and McWilliams 1990; Gent et al. 1995; Danabasoglu and McWilliams 1995; Hirst and McDougall 1996; Duffy et al. 1997, 1999; Bryan et al. 1999), and was largely eliminated by applying the eddy-induced tracer parameterization of Gent and McWilliams (1990) (the GM parameterization), which replaces the unphysical horizontal tracer mixing by along-isopycnal tracer diffusion and advection. This measure led to many desirable features, such as a much more realistic representation of AAIW and deep-water properties.

Our focus is on a more realistic representation of the latter by an alternative method, namely replacing the convective adjustment parameterization by a more physically based scheme. Since the detrimental effect of horizontal mixing is expected to be strongest where fronts

occur, such as associated with the ACC and AAIW formation, we do not expect to yield any improvements there. However, most of the initial excessive open-ocean convection encountered in our model occurred in the SO south of the ACC, especially in the central Weddell Sea and Ross Sea gyres, where isopycnal surfaces are only moderately inclined relative to the level surface. We thus believe that this regional, high-latitude problem is actually associated with the crude convection parameterization rather than with the flaws of horizontal mixing.

Another motivation for this approach stems from the hypothesis that with applying isopycnal tracer diffusion and advection vigorously in regions where eddy activity is weak (see Bryan et al. 1999), the actual composition of source water masses to form NADW or AABW may become distorted. For example, in both Hirst and McDougall (1996) and Duffy et al. (1999), it is indicated that their deep ocean gets substantially colder and saltier upon switching to the GM parameterization (in Duffy et al. 1999 even far beyond observed estimates), and thus denser. At the same time, convection drops to practically zero. While a colder and fresher deep ocean would be indicative of stronger AABW formation, mainly as a product of relatively warm and salty LCDW being mixed with very cold but somewhat fresher shelf water (e.g., Whitworth et al. 1998; Orsi et al. 1999), colder and saltier deep water rather indicates diffusive cooling of CDW. The initial warm and fresh bias in Hirst and McDougall (1996) and Duffy et al. (1999) indeed seemed to have been associated with diapycnal mixing of SH subtropical water into subpolar waters, creating unphysical instabilities along wide areas of frontal zones. Combined with the crude convective adjustment parameterization, relatively warm and fresh surface water is effectively transformed to the deep ocean, thereby making the deep ocean overall less dense than observed. This does not seem to be a major problem in our reference simulation, where the deep ocean is too cold and too fresh, but compensates in density, even without the GM parameterization.

On the other hand, we realize that in an attempt to simulate the real world, one should consider both the dynamic effect of mesoscale eddies of mixing vertical stability gradients (e.g., Bryan et al. 1999) and mesoscale convective mixing arising from large-scale preconditioning in high latitudes (e.g., Marshall and Schott 1999; Hirst and Cai 1994). The prerequisite here would be that available potential energy be not exclusively removed by excessive ''eddy activity'' (proportional to the ''bolus velocity'') in high latitudes. This, however, seems to occur in simulations where the ''mixing coefficient'' associated with the GM parameterization is not carefully chosen (Bryan et al. 1999; Visbeck et al. 1997; England and Rahmstorf 1999). Accordingly, in most of the studies referenced above investigating the impact of the GM parameterization, the chosen mixing coefficient (a constant 1000 $m^2\ s^{-1}$) seems indeed inappropriate for high latitudes beyond the polar front.

5. Summary and conclusions

Using a coarse-resolution version of the HOPE OGCM, we first reduced convection by adjusting the frequency of convective adjustments in the SO, limiting it to every ten days rather than every model time step (20 hours) (experiment SCN). Subsequently, a physically more consistent treatment was attempted by adopting the subgrid-scale penetrative plume convection scheme of Paluszkiewicz and Romea (1997). First, we applied this scheme only to the SO (experiment MIX), and then globally (PCN). Since experiment PCN involved a change in the North Atlantic overturning, the adjustment time for the deep ocean is longer. Due to the climate drift not having reached near-equilibrium (see section 2d) after 3000 years of integration, we did not analyze its results except for the strength of the convection itself. Based on the positive experience of our earlier study (KS), daily wind forcing over SO sea ice and a widened shelf topography in the Weddell Sea and the Ross Sea were retained.

Table 1 summarizes the results. When the conventional convection scheme is applied (REF), the deep ocean (4000 m) potential temperature and salinity are severely underestimated compared to Levitus (1982). However, when convection is reduced in an ad hoc or a more physical manner, globally averaged deep-ocean potential temperature and salinity increased remarkably close to the observed value under the influence of the associated overturning circulation.

Although the deep-ocean thermohaline properties increased by a comparable amount in both experiments, the reasons for the changes are different. In both SCN and MIX, the rate of the maximum SO convection decreased roughly by the same amount, about 30%, but the response of the overturning circulation cells appears to be substantially different. NADW outflow increased substantially in SCN, but the SO cell remained similar to that of REF, while MIX shows an opposite trend. This difference in the strength of the overturning cells is reflected in the meridional property sections. In SCN, the increased NADW outflow plays a major role in increasing the globally averaged deep-ocean potential temperature and salinity, but regional SO water mass properties are only moderately improved where the southward extension of LCDW is concerned. This seems to be mainly associated with too deep-reaching SO convection using the convective adjustment scheme, even though its frequency was reduced.

On the other hand, in MIX, the substantially reduced and shallower SO cell acts to pull the warm and saline CDW farther south close to the Antarctic continental margin, resulting in far more realistic deep-ocean potential temperature and salinity. Furthermore, SO sea ice thickness experienced a remarkable increase to ob-

served values and a rectification of its seasonal cycle. This suggests that the more physical plume convection scheme used in this study not only improves global-scale deep-ocean water mass properties, but also regional sea ice–ocean interactions, such as the magnitude and seasonality of vertical oceanic heat flux associated with convection, which in turn modifies sea ice. Furthermore, while the plume scheme reduces open-ocean convection substantially, it still maintains convection in the model's Labrador and GIN Seas (as demonstrated in PCN), consistent with large-scale observed evidence.

While we obtained far more realistic deep-ocean potential temperature and salinity (globally averaged within 0.15°C and 0.01 psu of the observed estimate), there are various other factors, such as the type of surface forcing, that could contribute to improving the deep-ocean properties. Also, while open-ocean convection is reduced significantly, it is still two to three orders of magnitude larger than what simulations with the GM parameterization suggest (see section 3a). Regardless of the latter, replacing the traditional convective adjustment scheme by a subgrid-scale plume convection parameterization, however, seems to be a very efficient and physically motivated approach. AAIW improved only marginally. A better representation of AAIW, however, was not targeted in this study. As outlined in section 1, the employment of the GM parameterization, or equivalent, is expected to be essential in reproducing AAIW more realistically.

Observations indicate that AABW is predominantly produced through near-boundary convection by a mixing of very cold and relatively saline shelf water with warmer and even saltier LCDW at the continental slope around Antarctica (Warren 1981; Killworth 1983, and references therein), while a small portion of it may be occasionally be produced by open-ocean convection (Marshall and Schott 1999). As a conclusion, this study proposes that in order to reproduce the deep-ocean properties more realistically, the strength in SO open-ocean convection should be substantially weakened, less deep penetrating, and seasonally phase adjusted by employing a physically motivated subgrid-scale convection parameterization such as the current plume convection scheme of Paluszkiewicz and Romea (1997). At the same time, this study, together with KS, suggests that the rate of near-boundary convection, which is not well represented in most OGCMs (including our case), should be enhanced through a more detailed (especially wide enough) representation of the continental shelves around Antarctica and high-quality wind fields including synoptic-scale variability to drive the SO sea ice pack.

Acknowledgments. Thanks are due to Terri Paluszkiewicz, who provided us with the plume convection code. Together with Eric Skyllingstad she also provided us with technical instructions as well as constructive remarks on an earlier draft of this paper. Various recommendations of two anonymous reviewers are appreciated; they broadened the scope of this paper toward a more general discussion about alternative methods on how to reduce spurious convection in OGCMs. This research is supported by NASA Grant NAG5-7751. The computations for this work were conducted on the Cray-J90 of the Texas A&M University Supercomputing Facility.

REFERENCES

Akitomo, K., 1999: Open-ocean deep convection due to thermobaricity. 1. Scaling argument. *J. Geophys. Res.,* **104** (C3), 5225–5234.

Arakawa, A., and V. R. Lamb, 1977: Computational design of the basic dynamical processes of the UCLA general circulation model. *Methods Comput. Phys.,* **17,** 173–265.

Brennecke, W., 1921: Die ozeanographischen Arbeiten der Deutschen Antarktischen Expedition 1911–1912. *Aus dem Archiv der Deutschen Seewarte,* Vol. 39, No. 1, 216 pp.

Broecker, W. S., 1997: Thermohaline circulation, the Achilles heel of our climate system: Will man-made CO_2 upset the current balance? *Science,* **278,** 1582–1589.

Bryan, K., J. K. Dukowicz, and R. D. Smith, 1999: On the mixing coefficient in the parameterization of bolus velocity. *J. Phys. Oceanogr.,* **29,** 2442–2456.

Cai, W., and R. J. Greatbatch, 1995: Compensation for the NADW outflow in a global ocean general circulation model. *J. Phys. Oceanogr.,* **25,** 226–241.

——, and P. G. Baines, 1996: Interactions between thermohaline- and wind-driven circulations and their relevance to the dynamics of the Antarctic Circumpolar Current in a coarse-resolution global ocean general circulation model. *J. Geophys. Res.,* **101** (C6), 14 073–14 093.

Callahan, J. E., 1972: The structure and circulation of deep water in the Antarctic. *Deep-Sea Res.,* **19,** 563–575.

Carmack, E. C., 1977: Water characteristics of the Southern Ocean south of Polar Front. *Voyage of Discovery,* M. Engel, Ed., *Deep-Sea Res.,* **24** (Suppl.), 15–41.

——, and P. D. Killworth, 1978: Formation and interleaving of abyssal water masses off Wilkes Land, Antarctica. *Deep-Sea Res.,* **25,** 357–369.

Cavalieri, D. J., and S. Martin, 1985: A passive microwave study of polynyas along the Antarctic Wilkes Land coast. *Oceanology of the Antarctic Continental Shelf,* S. S. Jacobs, Ed. Antarctic Research Series, Vol. 43, Amer. Geophys. Union, 227–252.

Clarke, R. A., and J.-C. Gascard, 1983: The formation of Labrador Sea Water. Part I: Large-scale processes. *J. Phys. Oceanogr.,* **13,** 1764–1778.

Cummins, P. F., G. Holloway, and A. E. Gargett, 1990: Sensitivity of the GFDL ocean general circulation model to a parameterization of vertical diffusion. *J. Phys. Oceanogr.,* **20,** 817–830.

Danabasoglu, G., and J. C. McWilliams, 1995: Sensitivity of the global ocean circulation to parameterizations of mesoscale tracer transports. *J. Climate,* **8,** 2967–2987.

Delworth, T., S. Manabe, and R. J. Stouffer, 1993: Interdecadal variations of the thermohaline circulation in a coupled ocean–atmosphere model. *J. Climate,* **6,** 1993–2011.

Denbo, D. W., and E. D. Skyllingstad, 1996: An ocean large eddy model with application to convection in the Greenland Sea. *J. Geophys. Res.,* **101,** 1095–1110.

Doney, S. C., W. G. Large, and F. O. Bryan, 1998: Surface ocean fluxes and water mass transformation rates in the coupled NCAR climate system model. *J. Climate,* **11,** 1420–1441.

Drijfhout, S., C. Heinze, M. Latif, and E. Maier-Reimer, 1996: Mean circulation and internal variability in an ocean primitive equation model. *J. Phys. Oceanogr.,* **26,** 559–580.

Duffy, P. B., and K. Caldeira, 1997: Sensitivity of simulated salinity

in a three-dimensional ocean model to upper ocean transport of salt from sea ice formation. *Geophys. Res. Lett.*, **24** (11), 1323–1326.

——, ——, J. Selvaggi, and M. Hoffert, 1997: Effects of subgrid-scale mixing parameterizations on simulated distributions of natural ^{14}C, temperature, and salinity in a three-dimensional ocean general circulation model. *J. Phys. Oceanogr.*, **27,** 498–523.

——, M. Eby, and A. J. Weaver, 1999: Effects of salt rejected during formation of sea ice on results of a global ocean–atmosphere–sea ice climate model. *Geophys. Res. Lett.*, **26** (12), 1739–1742.

England, M. H., 1993: On the formation of global-scale water masses in ocean general circulation models. *J. Phys. Oceanogr.*, **23,** 1523–1552.

——, and S. Rahmstorf, 1999: Sensitivity of ventilation rates and radiocarbon uptake to subgrid-scale mixing in ocean models. *J. Phys. Oceanogr.*, **29,** 2802–2827.

Fichefet, T., S. Hovine, and J.-C. Duplessy, 1994: A model study of the Atlantic thermohaline circulation during the last glacial maximum. *Nature,* **372,** 252–255.

Fieux, M., C. Andrié, P. Delecluse, A. G. Ilahude, A. Kartavtseff, F. Mantisi, R. Molcard, and J.C. Swallow, 1994: Measurements within the Pacific–Indian Oceans throughflow region. *Deep-Sea Res.*, **41,** 1091–1130.

Flato, G. M., G. J. Boer, W. G. Lee, N. A. McFarlane, D. Ramsden, M. C. Reader, and A. J. Weaver, 2000: The Canadian Center for Climate Modelling and Analysis global coupled model and its climate. *Climate Dyn.*, **16,** 451–467.

Foster, T. D., and E. C. Carmack, 1976: Frontal zone mixing and Antarctic Bottom Water formation in the southern Weddell Sea. *Deep-Sea Res.*, **23,** 301–317.

Gent, P. R., and J. C. McWilliams, 1990: Isopycnal mixing in ocean circulation models. *J. Phys. Oceanogr.*, **20,** 150–155.

——, J. Willebrand, T. J. McDougall, and J. C. McWilliams, 1995: Parameterizing eddy-induced transports in ocean circulation models. *J. Phys. Oceanogr.*, **25,** 463–474.

Gill, A. E., 1973: Circulation and bottom water production in the Weddell Sea. *Deep-Sea Res.*, **20,** 111–140.

Gloersen, P., W. J. Campbell, D. J. Cavalieri, J. C. Comiso, C. L. Parkinson, and H. H. Zwally, 1992: Arctic and Antarctic sea ice, 1978–1987: Satellite passive-microwave observations and analysis. NASA Spec. Publ., 511, 290 pp. [Available from Laboratory for Hydrospheric Processes, NASA Goddard Space Flight Center, Greenbelt, MD 20771.]

Goosse, H., 1997: Modelling the large-scale behavior of the coupled ocean–sea ice system. Ph.D. dissertation, Université Catholique de Louvain, 231 pp. [Available from Université Catholique de Louvain, Louvain-la-Neuve, Belgium.]

Gordon, A. L., 1974: Varieties and variability of Antarctic Bottom Water. *Colloque International sur les Processus de Formation des Eaux Oceaniques Profondes*, Paris, France, Colloq. Int. du Centre National de la Recherche Scientifique, Vol. 215, 33–47.

——, 1978: Deep Antarctic convection west of Maud Rise. *J. Phys. Oceanogr.*, **8,** 600–612.

——, 1986: Interocean exchange of thermocline water. *J. Geophys. Res.*, **91** (C4), 5037–5046.

——, 1998: Western Weddell Sea thermohaline stratification. *Ocean, Ice, and Atmosphere: Interactions at the Antarctic continental margin,* S. S. Jacobs and R. F. Weiss, Eds. Antarctic Research Series, Vol. 75, Amer. Geophys. Union, 215–240.

——, and P. Tchernia, 1972: Water of the continental margin off Adélie Coast, Antarctica. *Antarctic Oceanology II: The Australian-New Zealand Sector*, D. E. Hayes, Ed. Antarctic Research Series, Vol. 19, Amer. Geophys. Union, 59–69.

——, and B. A. Huber, 1990: Southern Ocean winter mixed layer. *J. Geophys. Res.*, **95** (C7), 11 635–11 672.

Hastenrath, S., 1982: On the meridional heat transports in the world ocean. *J. Phys. Oceanogr.*, **12,** 922–927.

Hellerman, S., and M. Rosenstein, 1983: Normal monthly wind stress over the world ocean with error estimates. *J. Phys. Oceanogr.*, **13,** 1093–1104.

Hibler, W. D., III, 1979: A dynamic and thermodynamic sea ice model. *J. Phys. Oceanogr.*, **9,** 815–846.

Hirst, A. C., and W. Cai, 1994: Sensitivity of a World Ocean GCM to changes in subsurface mixing parameterization. *J. Phys. Oceanogr.*, **24,** 1256–1279.

——, and T. J. McDougall, 1996: Deep-water properties and surface buoyancy flux as simulated by a *z*-coordinate model including eddy-induced advection. *J. Phys. Oceanogr.*, **26,** 1320–1343.

Hogg, N. G., G. Siedler, and W. Zenk, 1999: Circulation and variability at the southern boundary of the Brazil Basin. *J. Phys. Oceanogr.*, **29,** 145–157.

Hu, D., 1997: Global-scale water masses, meridional circulation, and heat transport simulated with a global isopycnal ocean model. *J. Phys. Oceanogr.*, **27,** 96–120.

Jacobs, S. S., R. G. Fairbanks, and Y. Horibe, 1985: Origin and evolution of water masses near the Antarctic continental margin: Evidence from $H_2{}^{18}O/H_2{}^{16}O$ ratios in sea water. *Oceanology of the Antarctic Continental Shelf*, S. S. Jacobs, Ed., Antarctic Research Series, Vol. 43, Amer. Geophys. Union, 59–85.

Killworth, P. D., 1979: On ''chimney'' formations in the ocean. *J. Phys. Oceanogr.*, **9,** 531–554.

——, 1983: Deep convection in the World Ocean. *Rev. Geophys.*, **21,** 1–26.

Kim, S.-J., 1995: The transition zone between the oceanic and shelf regimes around Antarctica. M.S. thesis, Dept. of Oceanography, Texas A&M University, 70 pp.

——, and A. Stössel, 1998: On the representation of the Southern Ocean water masses in an ocean climate model. *J. Geophys. Res.*, **103** (C11), 24 891–24 906.

Labrador Sea Group, 1998: The Labrador Sea Deep Convection Experiment. *Bull. Amer. Meteor. Soc.*, **79,** 2033–2058.

Large, W. G., G. Danabasoglu, and S. C. Doney, 1997: Sensitivity to surface forcing and boundary layer mixing in a global ocean model: Annual-mean climatology. *J. Phys. Oceanogr.*, **27,** 2418–2447.

Legutke, S., and R. Voss, 1999: The Hamburg Atmosphere–Ocean Coupled Circulation Model ECHO-G. Tech. Rep. 14, German Climate Computer Centre (DKRZ), Hamburg, Germany, 61 pp. [Available from Deutsches Klimarechenzentrum, Bundesstrasse 55, D-20146 Hamburg, Germany.]

——, E. Maier-Reimer, A. Stössel, and A. Hellbach, 1997: Ocean–sea ice coupling in a global ocean general circulation model. *Ann. Glaciol.*, **25,** 116–120.

Levitus, S., 1982: *Climatological Atlas of the World Ocean.* NOAA Prof. Paper No. 13, U.S. Govt. Printing Office, 173 pp. and 17 microfiche.

Lilly, J. M., P. B. Rhines, M. Visbeck, R. Davis, J. R. N. Lazier, F. Schott, and D. Farmer, 1999: Observing deep convection in the Labrador Sea during winter 1994/95. *J. Phys. Oceanogr.*, **29,** 2065–2098.

Macdonald, A. M., and C. Wunsch, 1996: An estimate of global ocean circulation and heat fluxes. *Nature,* **382,** 436–439.

Maier-Reimer, E., U. Mikolajewicz, and K. Hasselmann, 1993: Mean circulation of the Hamburg LSG OGCM and its sensitivity to the thermohaline surface forcing. *J. Phys. Oceanogr.*, **23,** 731–757.

Manabe, S., and R. J. Stouffer, 1996: Low-frequency variability of surface air temperature in a 1000-year integration of a coupled atmosphere–ocean–land surface model. *J. Climate,* **9,** 376–393.

Marshall, J., and F. Schott, 1999: Open-ocean convection: Observations, theory, and models. *Rev. Geophys.*, **37,** 1–64.

Martinson, D. G., 1990: Evolution of Southern Ocean winter mixed layer and sea ice: Open-ocean deep water formation and ventilation. *J. Geophys. Res.*, **95,** 11 641–11 654.

McCartney, M. S., 1977: Subantarctic Mode Water. *Voyage of Discovery.* M. Engel, Ed., *Deep-Sea Res.*, **24** (Suppl.), 43–84.

Molinelli, E., 1981: The Antarctic influence on the Antarctic Intermediate Water. *J. Mar. Res.*, **39,** 267–293.

Nakata, M., and N. Suginohara, 1998: Role of deep stratification in

transporting deep water from the Atlantic to the Pacific. *J. Geophys. Res.*, **103,** 1067–1086.

Oberhuber, J. M., 1993: Simulation of the Atlantic circulation with a coupled sea ice–mixed layer–isopycnal general circulation model. Part I: Model description. *J. Phys. Oceanogr.,* **23,** 808–829.

Orsi, A. H., T. Whitworth III, and W. D. Nowlin Jr., 1995: On the meridional extent and fronts of the Antarctic Circumpolar Current. *Deep-Sea Res.,* **42,** 641–673.

——, G. C. Johnson, and J. L. Bullister, 1999: Circulation, mixing, and production of Antarctic Bottom Water. *Progress in Oceanography,* Vol. 43, Pergamon, 55–109.

Owens, W. B., and P. Lemke, 1990: Sensitivity studies with a sea ice–mixed layer–pycnocline model in the Weddell Sea. *J. Geophys. Res.*, **95,** 9527–9538.

Paluszkiewicz, T., and R. D. Romea, 1997: A one-dimensional model for the parameterization of deep convection in the ocean. *Dyn. Atmos. Oceans,* **26,** 95–130.

Parkinson, C. L., and W. M. Washington, 1979: A large-scale numerical model of sea ice. *J. Geophys. Res.*, **84,** 311–337.

Pierce, D. W., K.-Y. Kim, and T. P. Barnett, 1996: Variability of the thermohaline circulation in an ocean general circulation model coupled to an atmospheric energy balance model. *J. Phys. Oceanogr.,* **26,** 725–738.

Price, J. F., and M. Baringer, 1994: Outflows and deep water production by marginal seas. *Progress in Oceanography,* Vol. 33, Pergamon, 161–200.

Redi, M. H., 1982: Oceanic isopycnal mixing by coordinate rotation. *J. Phys. Oceanogr.,* **12,** 1154–1158.

Reid, J. L., and R. J. Lynn, 1971: On the influence of the Norwegian–Greenland and Weddell Seas upon the bottom waters of the Indian and Pacific Oceans. *Deep-Sea Res.,* **18,** 1063–1088.

Rintoul, S. R., 1998: On the origin and influence of Adélie Land bottom water. *Ocean, Ice, and Atmosphere: Interactions at the Antarctic Continental Margin,* S. S. Jacobs and R. Weiss, Eds. Antarctic Research Series, Vol. 75, Amer. Geophys. Union, 151–171.

Roach, A. T., K. Aagaard, and F. Carsey, 1993: Coupled ice–ocean variability in the Greenland Sea. *Atmos.-Ocean,* **31,** 319–337.

Rudels, B., D. Quadfasel, H. Friedrich, and M.-N. Houssasi, 1989: Greenland sea convection in the winter of 1987–1988. *J. Geophys. Res.,* **94,** 3223–3227.

Schott, F., M. Visbeck, and J. Fischer, 1993: Observations of vertical currents and convection in the central Greenland Sea during the winter of 1988–1989. *J. Geophys. Res.,* **98,** 14 402–14 421.

Semtner, A. J., Jr., and R. M. Chervin, 1992: Ocean general circulation from a global eddy-resolving model. *J. Geophys. Res.,* **97,** 5493–5550.

Stammer, D., R. Tokmakian, A. Semtner, and C. Wunsch, 1996: How well does a ¼° global circulation model simulate large-scale oceanic observations? *J. Geophys. Res.,* **101,** 25 779–25 811.

Stocker, T. F., D. G. Wright, and W. S. Broecker, 1992: The influence of high-latitude surface forcing on the global thermohaline circulation. *Paleoceanography,* **7,** 529–541.

Stössel, A., 1992: Sensitivity of Southern Ocean sea ice simulations to different atmospheric forcing algorithms. *Tellus,* **44A,** 395–413.

——, and W. B. Owens, 1992: The Hamburg sea ice model. Modell Betreuungsgrupe Tech. Rep. 3, Deutsches Klimarechenzentrum, 61 pp. [Available from Max-Planck-Institut für Meteorologie, Bundesstrasse 55, D-2000 Hamburg 13, Germany.]

——, S.-J. Kim, and S. S. Drijfhout, 1998: The impact of Southern Ocean sea ice in a global ocean model. *J. Phys. Oceanogr.,* **28,** 1999–2018.

Talley, L. D., 1984: Meridional heat transport in the Pacific Ocean. *J. Phys. Oceanogr.,* **14,** 231–241.

Toggweiler, J. R., and B. Samuels, 1995: Effects of sea ice on the salinity of Antarctic Bottom Waters. *J. Phys. Oceanogr.,* **25,** 1980–1997.

Turner, J. S., 1973: *Buoyancy Effects in Fluids.* Cambridge University Press, 367 pp.

Visbeck, M., J. Marshall, and T. Haine, 1997: Specification of eddy transfer coefficients in coarse-resolution ocean circulation models. *J. Phys. Oceanogr.,* **27,** 381–402.

Wadhams, P., 1994: Sea ice thickness changes and their relation to climate. *The Polar Oceans and Their Role in Shaping the Global Environment, Geophys. Monogr. Ser.,* No. 85, Amer. Geophys. Union, 337–361.

Warren, B. A., 1981: Deep circulation of the World Ocean. *Evolution of Physical Oceanography,* B. A. Warren and C. Wunsch, Eds., The MIT Press, 6–41.

Washington, W. M., and G. A. Meehl, 1996: High-latitude climate change in global coupled ocean–atmosphere–sea ice model with increased atmospheric CO_2. *J. Geophys. Res.,* **101,** 12 795–12 801.

Weatherly, J. W., T. W. Bettge, and B. P. Briegleb, 1997: Simulation of sea ice in the NCAR climate system model. *Ann. Glaciol.,* **25,** 107–110.

——, B. P. Briegleb, and W. G. Large, 1998: Sea ice and polar climate in the NCAR CSM. *J. Climate,* **11,** 1472–1486.

Whitworth, T., III, and R. G. Peterson, 1985: Volume transport of the Antarctic circumpolar current from bottom pressure measurements. *J. Phys. Oceanogr.,* **15,** 810–816.

——, and W. D. Nowlin Jr., 1987: Water masses and currents of the Southern Ocean at the Greenwich Meridian. *J. Geophys. Res.,* **92,** 6462–6476.

——, A. H. Orsi, S.-J. Kim, W. D. Nowlin Jr., and R. A. Locarnini, 1998: Water masses and mixing near the Antarctic Slope Front. *Ocean, Ice, and Atmosphere: Interations at the Antarctic Continental Margin,* S. S. Jacobs and R. Weiss, Eds. Antarctic Research Series, Vol. 75, Amer. Geophys. Union, 1–27.

Wolff, J., E. Maier-Reimer, and S. Legutke, 1997: The Hamburg Ocean Primitive Equation Model (HOPE). Modell Beratungsgruppe Tech. Rep. 13, Deutsches Kimarechenzentrum, 98 pp. [Available from Max-Planck-Institut für Meteorologie, Bundesstrasse 55, D-20146 Hamburg, Germany.]

Woodruff, S. D., R. J. Slutz, R. L. Jenne, and P. M. Streurer, 1987: A comprehensive ocean–atmosphere dataset. *Bull. Amer. Meteor. Soc.,* **68,** 1239–1250.

Worby, A. P., N. L. Bindoff, V. I. Lytle, I. Allison, and R. A. Masson, 1996: Winter ocean/sea ice interactions studied in the east Antarctic. *Eos, Trans. Amer. Geophys. Union,* **77**(46), 456–457.

Zwally, H. J., J. C. Comiso, and A. L. Gordon, 1985: Antarctic offshore leads and polynyas and oceanographic effects. *Oceanology of the Antarctic Continental Shelf,* S. S. Jacobs, Ed. Antarctic Research Series, Vol. 43, Amer. Geophys. Union, 203–226.